

# Dynamics of Thermocapillary-Driven Motion of Liquid Drops

Rachid Chebbi\*

Cite This: *ACS Omega* 2023, 8, 37196–37201

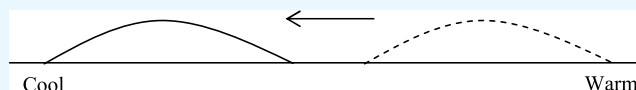
Read Online

ACCESS |

Metrics &amp; More

Article Recommendations

**ABSTRACT:** The thermocapillary migration of a drop placed on a solid plate is examined. The Brochard model using the lubrication approximation provides both Marangoni and Poiseuille flow components. The present 2D model extends Brochard analysis and provides a solution for the dynamics of drop migration using extended boundary conditions at the advancing and receding contact lines to account for both Marangoni and Poiseuille flow components, derived approximate drop profiles, and conservation of mass. The model is analytical, and the results are presented in a dimensionless form. The effects of the temperature gradient, surface tension coefficient to surface tension ratio, liquid viscosity, and static advancing and receding contact angles on migration dynamics are analyzed.



## 1. INTRODUCTION

Marangoni flows are driven by gradients in surface tension along the free liquid surface due to differences in temperature or composition. Marangoni flows have several applications including microfluidics, extraction processes, and tribology.<sup>1,2</sup> In thermocapillary migration of drops on heated plates, migration occurs from the hot side to the cold side in the direction of decreasing surface tension. Previous work related to migration over solid substrates is addressed in refs 2–8.<sup>2–8</sup> Such flows involve moving advancing and receding contact lines. Knowing their dynamics is essential in modeling drop migration. The dynamics of moving contact lines are characterized by singularity at the leading edge for hydrodynamic models, with unbounded viscous dissipation at the contact line as indicated in a previous study.<sup>9</sup> Huh and Scriven<sup>9</sup> explored the use of dynamic conditions including slip and long-range interaction forces in relation to the singularity at the moving contact line. Reviews of the dynamics of contact lines can be found in Dussan,<sup>10</sup> de Gennes,<sup>11</sup> Blake,<sup>12</sup> and the references therein. The different approaches taken include (i) a molecular-kinetic theory approach based on the Eyring concept,<sup>13</sup> (ii) a hydrodynamic approach using the slip condition near the leading edge,<sup>14,15</sup> and (iii) a relation between the dynamic contact angle and the contact line velocity, limiting the hydrodynamic approach to a distance above a cut-off level of molecular size.<sup>4,16</sup> In the case of perfect wetting, the hydrodynamic approach includes molecular interactions between the solid and the liquid using the disjoining pressure concept.<sup>17–19</sup> The approach used in ref 19 to solve the dynamics of spreading of a drop was found to yield results in very good agreement with experimental data obtained using different techniques, including those in ref 18.<sup>18</sup>

Greenspan<sup>3</sup> addressed the case of drop migration driven by the concentration gradient along the drop surface and used a dynamic contact angle condition based on a linear relation between the contact line velocity and the deviation of the

dynamic contact angle from the equilibrium contact angle. The dynamic contact angle condition in Brochard<sup>4</sup> and Brochard and de Gennes<sup>16</sup> was found based on a hydrodynamic approach using the lubrication theory approximation and viscous dissipation argument with integration performed near the contact line down to a point where the distance is of molecular size. Most viscous dissipation is considered to occur near the advancing and receding contact lines for the circular wedge migration. Brzoska et al.<sup>5</sup> considered the case of small drops moving on nonwetttable surfaces. They found experimentally that drop migration requires the drop radius to exceed a critical value with a velocity proportional to the drop radius and the temperature gradient. Ford and Nadim<sup>6</sup> investigated migration of a long wedge assumed infinite in length as an approximation and provided an expression for the steady-state migration velocity as a function of slip length and a steady-state thickness profile. The use of the migration velocity expression in ref 6 requires determination of the drop thickness profile. Smith<sup>7</sup> used a dynamic contact angle condition in which a power-law form relates the contact line velocity to the deviation of the dynamic contact angle from the equilibrium one. Smith reached the conclusion that two steady-state cases are possible: no motion and steady migration velocity. Dai et al.<sup>2</sup> considered the migration of a wedge of uniform drop thickness, except near the edges (pancake configuration), and compared the model with their experimental data for migration velocity, using measured values for volume to area ratios to get the assumed uniform oil thickness values as motion proceeds. Dai et al. experimental

Received: July 6, 2023

Accepted: September 15, 2023

Published: September 29, 2023



data<sup>2</sup> show that migration velocity is enhanced at a lower viscosity and higher temperature gradient (in magnitude). Pratap et al.<sup>8</sup> used a hydrodynamic model limited to a distance of molecular size from the moving contact line, estimated based on molecular dynamics simulations to derive an expression for the migration velocity assuming a circular footprint and a spherical cap drop. The results were found to underestimate the experimental data determined in ref 8.<sup>8</sup>

In more recent investigations, thermocapillarity has been used for processing polymer–nanoparticle composites<sup>20</sup> and fabrication of micro and nanostructures.<sup>21</sup> The thermal gradients used are mainly classified into longitudinal and transverse.<sup>20</sup> A simulation of a thin liquid drop deposited on a cool plate below a warm plate is shown to deform and reach equilibrium.<sup>21</sup> At a large temperature difference and Marangoni number exceeding the critical value, the drop deforms and the maximum height increases until it touches the top plate protrusion.<sup>21</sup> The numerical results<sup>21</sup> are validated against Xie et al.<sup>22</sup> experimental data for drop migration in a microgravity environment. The analysis shows the need to account for inertia terms for Reynolds numbers larger than one.<sup>21</sup> Muñoz et al. model and numerical results<sup>23</sup> show that combining thermocapillarity, by subjecting a drop surface to a Gaussian temperature distribution, with surface acoustic waves (SAW) atomization reduces aerosol droplets' diameter and work input, with slip on the solid surface reducing the rupture time. When imposing a radial temperature gradient on a drop placed on a horizontal surface, spreading occurs first, followed by ring migration as shown in the numerical model results of Ma et al.<sup>24</sup> Ring-like motion was observed experimentally by Dai et al.<sup>25</sup> Confining wettability in a symmetric and rectangular hydrophilic zone is shown to expel fluid once the advancing contact line touches the hydrophobic zone borders.<sup>24</sup> The ultimate splitting of the drop suggests that the method can be a compelling substitute to other methods.<sup>24</sup>

Chebbi<sup>26,27</sup> used Brochard-de Gennes dynamic boundary conditions<sup>4,16</sup> to model the partial wetting of drops on the solid surface using (i) an analytical approach assuming a nearly circular profile<sup>27</sup> and (ii) a numerical approach to account for deviations from the spherical cap.<sup>26</sup> Both approaches gave very close results with good agreement with experimental data from three different publications, including data from Hocking and Rivers.<sup>14</sup> In the present model, the 2D planar model for the Brochard velocity profile<sup>4</sup> is used. We extend the Brochard-de Gennes boundary conditions<sup>4,16,28</sup> at the dynamic and receding contact lines for the case of Poiseuille flow to account for the additional Marangoni flow component, derive an approximate drop profile, and use the conservation of mass condition in order to solve for the dynamics of drop migration. The governing equations are presented first, followed by extended boundary condition derivation, approximate drop profile determination, solution and procedure, results and discussion, and conclusions.

## 2. COMPUTATIONAL METHODS

**2.1. Governing Equations.** We consider the case of a drop of cylindrical shape. A schematic of the cross section is shown in Figure 1 where  $x$  and  $z$  denote horizontal and vertical coordinates, respectively,  $\theta_A$  and  $\theta_B$  represent the left and right dynamic contact angles, respectively,  $\eta$  ranges from 0 to  $a$ , and  $\chi$  ranges from 0 to  $b$  in a reference system moving with the migrating drop, with both  $\eta$  and  $\chi$  measured from a point where the slope of the thickness profile is zero and the drop thickness is maximum.

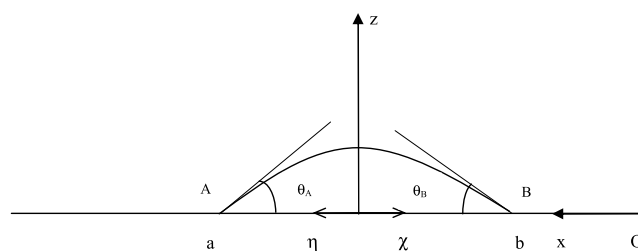


**Figure 1.** Schematic of a migrating drop (cylindrical wedge) moving from right to left (warm side to cool side).

For a thick drop, gravity causes flattening and gives a pancake shape to the drop.<sup>4</sup> We consider the case of a thin drop (cylindrical ridge). This restricts the drop dimension in the direction of drop migration,  $w$  (equal to  $x_A - x_B$ ) to be smaller than the Laplace length (defined as  $\sqrt{\sigma/\rho g}$  where  $\sigma$ ,  $\rho$ , and  $g$  denote surface tension and density of the liquid and acceleration of gravity, respectively).<sup>4</sup> We consider the case of partial wetting. The solid is subject to a uniform and longitudinal temperature gradient. Temperature is assumed independent of  $z$  given the small thickness of the drop.<sup>2</sup> Liquid density changes are neglected, and the fluid is assumed Newtonian. Using the lubrication theory approximation (requiring relatively small contact angles), and assuming small velocities, we can neglect inertia terms with the Navier–Stokes equations reducing to

$$\frac{\partial p}{\partial z} = 0 \quad (1)$$

$$\frac{\partial p}{\partial x} = \mu \frac{\partial^2 v}{\partial z^2} \quad (2)$$

where  $p$  denotes pressure, and  $v$  is the liquid velocity measured in a coordinate system moving with the migrating liquid drop at a velocity  $U$  with respect to a fixed reference system originating at  $O$ .

The two boundary conditions at the gas–liquid and solid–liquid interfaces are

$$atz = h, \mu \frac{\partial v}{\partial z} = \frac{\partial \sigma}{\partial x} \quad (3)$$

$$atz = 0, v = -U \quad (4)$$

where  $h$  denotes the liquid thickness and  $\mu$  represents the liquid viscosity. Equation 4 expresses the no slip boundary condition in the moving reference system. We assume temperature  $T$  independent of  $z$ , in addition to the uniform temperature gradient  $T_x$  and a constant surface tension temperature gradient,  $\sigma_T$ . Using the chain rule yields the surface tension gradient induced by the temperature gradient.

$$\frac{\partial \sigma}{\partial x} = \sigma_T T_x \quad (5)$$

Using eqs 1–5 gives<sup>2,4</sup>

$$v = \frac{1}{\mu} \left[ \sigma_T T_x z + \frac{1}{2} \frac{dp}{dx} (z^2 - 2zh) \right] - U \quad (6)$$

There is no net volumetric flow rate through any cross section. This yields<sup>2,4</sup>

$$\frac{dp}{dx} = -\frac{3\mu U}{h^2} + \frac{3}{2h} \sigma_T T_x \quad (7)$$

Applying Newton's second law and the zero flux condition, while using the expression for the capillary driving force,<sup>4</sup> gives

$$m \frac{dU}{dt} = -l \int_{x_B+\varepsilon}^{x_A-\varepsilon} \tau_w dz + l(\sigma_{SG,A} - \sigma_{SL,A}) - l(\sigma_{SG,B} - \sigma_{SL,B}) \quad (8)$$

where  $t$  is the time,  $l$  denotes the wedge dimension in the transverse direction to migration,  $\varepsilon$  is of molecular size,  $m$  is the droplet mass, and  $\sigma_{SG,A}$  and  $\sigma_{SL,A}$  represent the solid–gas and solid–liquid interfacial tensions at A with similar notations used at B, respectively. The wall shear stress is given by

$$\tau_w = \mu \left. \frac{\partial v}{\partial z} \right|_{z=0} \quad (9)$$

Using the Young–Dupré equation and neglecting the inertia term reduces eq 8 to

$$-l \int_{x_B+\varepsilon}^{x_A-\varepsilon} \tau_w dx + l(\sigma_A \cos \theta_{A,e} - \sigma_B \cos \theta_{B,e}) = 0 \quad (10)$$

where subscript e refers to equilibrium values.

**2.2. Viscous Dissipation and Contact Angle Correlations.** We define  $\bar{x}$  as the distance from the right contact line ( $x_A - x$ ). Near the contact line and for  $\bar{x}$  as low as  $\varepsilon$  and as high as  $\bar{x}_m$ , the profile near contact line A is approximated as linear (wedge profile).

$$\frac{d\Phi_v}{d\bar{x}} = l \int_0^h \mu \left( \frac{\partial v}{\partial z} \right)^2 dz; h = \theta \bar{x} \quad (11)$$

where  $\Phi_v$  is the rate of viscous dissipation.

Differentiating eq 6 gives

$$\frac{\partial v}{\partial z} = \frac{1}{\mu} \left[ \sigma_T T_x + \frac{dp}{dx} (z - h) \right] \quad (12)$$

Then substituting into eq 11 and integrating yields, after substitution of the pressure gradient expression using eq 7 and simplification

$$\frac{d\Phi_v}{d\bar{x}} = \frac{l}{\mu} \left[ \frac{h}{4} (\sigma_T T_x)^2 + 3 \frac{\mu^2 U^2}{h} \right] \quad (13)$$

The second term is predominant near the contact line where  $h$  is small. Neglecting the first term in eq 13 and integrating yields

$$\Phi_v = 3l \frac{\mu U^2}{\theta} \Gamma; \Gamma = \ln \left( \frac{\bar{x}_m}{\varepsilon} \right) \quad (14)$$

Equating  $\Phi_v$  with the work term  $l\sigma(\cos \theta_e - \cos \theta)U$  gives at the advancing contact line A

$$U = \frac{\sigma(\cos \theta_{A,e} - \cos \theta_A)}{3\mu\Gamma} \approx \frac{\sigma\theta_A(\theta_A^2 - \theta_{A,e}^2)}{6\mu\Gamma} \quad (15)$$

Equating  $\Phi_v$  with the work term  $l\sigma(\cos \theta - \cos \theta_e)U$  gives at the receding contact line B

$$U = \frac{\sigma\theta_B(\cos \theta_B - \cos \theta_{B,e})}{3\mu\Gamma} \approx \frac{\sigma\theta_B(\theta_{B,e}^2 - \theta_B^2)}{6\mu\Gamma} \quad (16)$$

This shows that the dynamic contact angle condition in refs 4,16,28 also applies to the variable surface tension gradient case considered here as a good approximation.

**2.3. Dynamics of Drop Migration.** Outside a small region near the advancing contact line, the drop profile, assumed as approximately circular (Figure 1), is given by

$$\text{lower temperature side: } h_A = \frac{\theta_A}{2a}(a^2 - \eta^2) \quad (17)$$

The profile satisfies the following boundary conditions

$$\text{at } \eta = a, h_A = 0 \text{ and } \frac{dh_A}{d\eta} = -\theta_A \quad (18)$$

$$\text{at } \eta = 0, \frac{dh_A}{d\eta} = 0 \quad (19)$$

In the same way we have

$$\text{higher temperature side: } h_B = \frac{\theta_B}{2b}(b^2 - \chi^2) \quad (20)$$

The profile satisfies the following boundary conditions

$$\text{at } \chi = b, h_B = 0 \text{ and } \frac{dh_B}{d\chi} = -\theta_B \quad (21)$$

$$\text{at } \chi = 0, \frac{dh_B}{d\chi} = 0 \quad (22)$$

The shear force term in eq 10 is split into two terms.

$$l \int_{x_B+\varepsilon}^{x_A-\varepsilon} \tau_w dx = l \int_0^{a-\varepsilon} \tau_w d\eta + l \int_0^{b-\varepsilon} \tau_w d\chi \quad (23)$$

where integration excludes two regions very near the contact lines (within  $\varepsilon$ ) in which continuum mechanics is no longer applicable with the present model. Integrating both terms using eqs 7, 12, 17, 20 gives

$$w \int_{x_B+\varepsilon}^{x_A-\varepsilon} \tau_w dx = l \frac{3\mu U}{\theta_A} \ln \left( \frac{2a - \varepsilon}{\varepsilon} \right) + l \frac{3\mu U}{\theta_B} \ln \left( \frac{2b - \varepsilon}{\varepsilon} \right) - w l \frac{\sigma_T T_x}{2} \quad (24)$$

Then substituting into the force balance eq 10 gives after approximating the logarithmic terms as  $\Gamma$

$$\frac{3\mu U}{\theta_A} \Gamma + \frac{3\mu U}{\theta_B} \Gamma - \frac{\sigma_T T_x}{2} w = \sigma_A \cos \theta_{A,e} - \sigma_B \cos \theta_{B,e} \quad (25)$$

In addition, the conservation of mass equation yields

$$\frac{V}{l} = \int_0^a h_a d\eta + \int_0^b h_b d\chi \quad (26)$$

where  $V$  is the liquid drop volume, assumed constant. Substituting eqs 17 and 20 into eq 26 provides after integration

$$\frac{V}{l} = \frac{\theta_A a^2}{3} + \frac{\theta_B b^2}{3} \quad (27)$$

Using the continuity of the lower and higher temperature profiles at the origin

$$\text{at } \eta = \chi = 0, h_A = h_B \quad (28)$$

along with

$$a + b = w \quad (29)$$

yields

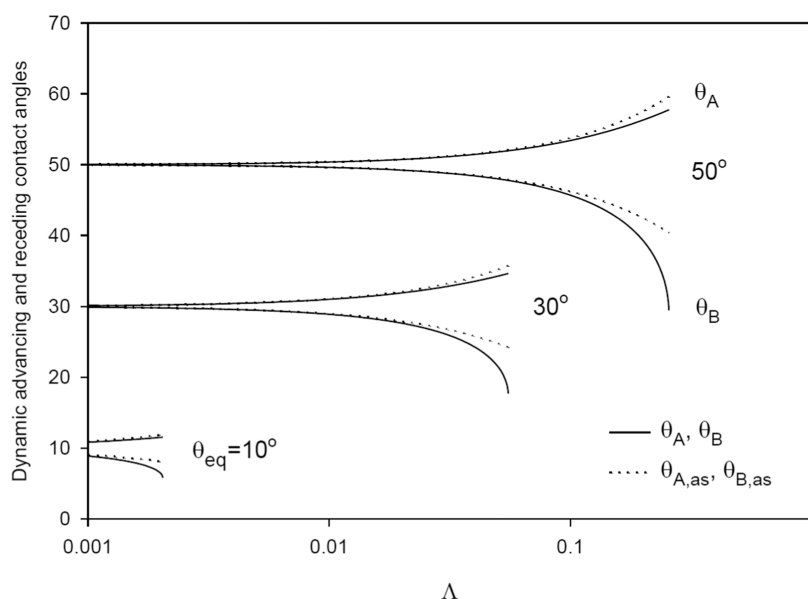


**Figure 2.** Plots of advancing and receding contact angles versus  $\Lambda$  for  $\theta_e = 10, 30,$  and  $50^\circ$  (small contact angle hysteresis effect case).

$$a = \frac{\theta_B}{\theta_A + \theta_B} w; b = \frac{\theta_A}{\theta_A + \theta_B} w \quad (30)$$

Substituting for  $a$  and  $b$  into eq 27 gives

$$3V = lw^2 \frac{\theta_A \theta_B}{\theta_A + \theta_B} \text{ or } \frac{3}{\zeta} V = w^3 \frac{\theta_A \theta_B}{\theta_A + \theta_B} \quad (31)$$

with  $\zeta$  defined as  $l/w$ .

**2.4. Solution Procedure.** The solution can be reached by using the following steps: (i) guess  $U$ , (ii) calculate  $\theta_A$  and  $\theta_B$ , assuming a constant logarithm term, denoted as  $\Gamma$  and using the following expressions obtained from the cubic eqs 15 and 16, respectively

$$\theta_A = \frac{2}{\sqrt{3}} \theta_{A,e} \cos \left[ \frac{1}{3} \arccos \left( \frac{3^{3/2} \Lambda}{2\theta_{A,e}^3} \right) \right] \quad (32)$$

$$\theta_B = \frac{2}{\sqrt{3}} \theta_{B,e} \cos \left[ \frac{1}{3} \arccos \left( -\frac{3^{3/2} \Lambda}{2\theta_{B,e}^3} \right) \right] \quad (33)$$

where  $\Lambda$  is defined as  $6\Gamma Ca$ , and  $Ca$  denotes the capillary number  $\mu U/\sigma$ .

Defining  $\theta_e$  and contact angle hysteresis  $\delta^{28}$  as

$$\cos \theta_e = (\cos \theta_{Ae} + \cos \theta_{Be})/2; \delta = \cos \theta_{Be} - \cos \theta_{Ae} \quad (34)$$

and substituting into eq 25 gives

$$\begin{aligned} \frac{3\mu U}{\theta_A} \Gamma + \frac{3\mu U}{\theta_B} \Gamma &= \Delta \sigma \left( \frac{1}{2} + \cos \theta_e \right) - \sigma \delta; \\ \Delta \sigma &= \sigma_A - \sigma_B = w \sigma_T T_x; \\ \sigma &= (\sigma_A + \sigma_B)/2 \end{aligned} \quad (35)$$

Considering the case of small static contact angle hysteresis  $\delta$  and combining eqs 31 and 34 to eliminate  $w$  yields the following equation.

$$f(\Lambda) = \frac{\Lambda}{1 + 2\cos \theta_e \left( \frac{1}{\theta_A} + \frac{1}{\theta_B} \right)^{2/3}} = \frac{\sigma_T T_x}{\sigma} \left( \frac{3}{\zeta} V \right)^{1/3} \quad (36)$$

where  $\theta_A$  and  $\theta_B$  are functions of  $\Lambda$ . The solution is by trial and error and provides  $\Lambda$ , then  $\theta_A$  and  $\theta_B$  by substituting for  $\Lambda$  into eqs 32 and 33, and the migration velocity  $U$  using

$$U = \frac{\sigma}{6\mu\Gamma} \Lambda \quad (37)$$

Using eqs 15 and 16 yields the following asymptotic solutions as  $\Lambda$  tends to zero.

$$\theta_{A,as} \approx \theta_{A,e} \left( 1 + \frac{\Lambda}{2\theta_{A,e}^3} \right); \theta_{B,as} \approx \theta_{B,e} \left( 1 - \frac{\Lambda}{2\theta_{B,e}^3} \right) \quad (38)$$

Integration yields

$$x_B = \int_0^t U dt; x_A = x_B + w \quad (39)$$

where  $U$  varies with  $x$  and the right edge position  $x_B$  is selected as zero at  $t$  equals to 0.

For a constant gradient in surface tension, surface tension is obtained as

$$\sigma = \sigma_i + \sigma_T T_x x_B; \sigma_i = \sigma_r + \sigma_T (T_i - T_r) \quad (40)$$

$\mu$  is a function of temperature  $T$  at  $x_B$

$$T = T_i + T_x x_B \quad (41)$$

We can simply use numerical integration of eq 39

$$\Delta x_B = U \Delta t \quad (42)$$

### 3. RESULTS AND DISCUSSION

The results are given in graphical forms for the case  $\delta \cong 0$  (zero or negligible static contact angle hysteresis). The advancing and receding contact angles  $\theta_A$  and  $\theta_B$  are plotted versus  $\Lambda$  for  $\theta_e = 10, 30,$  and  $50^\circ$  (Figure 2). The arguments of the arccosine function are restricted not to exceed one in absolute value. This limits the range for  $\Lambda$  for each selected value of the equilibrium

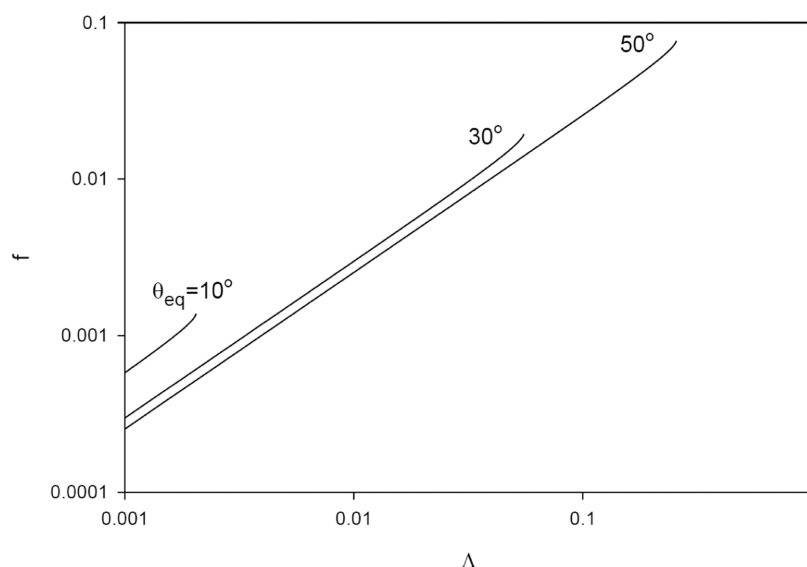


**Figure 3.** Plots of  $f$  defined in eq 36 versus  $\Lambda$  for  $\theta_e = 10, 30,$  and  $50^\circ$  (small contact angle hysteresis effect case).

contact angle. The advancing contact angle  $\theta_A$  is found to increase with the increasing capillary number, while  $\theta_B$  decreases with the increasing capillary number,  $Ca = \Lambda/(6\Gamma)$ . The asymptotic solutions are seen to be good estimates in a major part of the full range of values of  $\Lambda$  with a wider range of validity in the case of  $\theta_A$ . Furthermore, the asymptotic solution  $\theta_{A,as}$  is found to overestimate the dynamic advancing contact angle, while  $\theta_{B,as}$  underestimates the dynamic receding contact angle.

Figure 3 shows plots of  $f$  versus  $\Lambda$  for different values of  $\theta_e$ . As seen from Figure 3,  $f$  increases with the increasing capillary number and/or decreasing equilibrium contact angle. Using eq 36, we conclude that  $Ca$  increases as volume  $V$ , absolute value of temperature gradient  $|T_x|$ , and/or  $|\sigma_T|/\sigma$  increase. Furthermore, for specific values of  $V$ ,  $|T_x|$ ,  $|\sigma_T|$ , and  $\sigma$ , migration velocity is inversely proportional to absolute viscosity  $\mu$ . Using Figures 2 and 3 shows that for a given value of  $\theta_e$ ,  $\theta_A$  increases and  $\theta_B$  decreases with increasing volume  $V$ ,  $|T_x|$ , and/or  $|\sigma_T|/\sigma$ .

Instead of using a numerical iterative procedure to solve the problem (eq 35), it is possible to solve the migration dynamics problem graphically. Substituting for the values of  $V$ , surface tension coefficient, temperature gradient, and  $\zeta$  in eq 35 provides the value of the  $f$ . Next, using Figure 2 provides the value of  $\Lambda$  and the values of  $\theta_A$  and  $\theta_B$  using the determined value of  $\Lambda$  (Figure 3).

#### 4. CONCLUSIONS

The present model extends the treatment of Brochard<sup>4</sup> and provides a solution for the dynamics of drop migration. The dynamic contact angle relation derived in the case of Poiseuille flow in refs 4,16,28 is shown to remain applicable in the case where flow involves a Marangoni flow component in addition to the Poiseuille flow one. The model can be used to solve unsteady-state migration as an approximation, given the slow migration dynamics. The effects of thermal gradient and viscosity changes on the dynamics of migration in the present investigation are found consistent with the experimental observations in ref 2.<sup>2</sup> Fully documented experimental data including equilibrium contact angle data as a function of temperature for the case of uniform, longitudinal, and unidirectional temperature gradients are required for comparison with the present model. For the case of liquid drops, the 2D

planar model is an approximation, as the problem is strictly speaking three-dimensional. The present treatment is an approximation to a complex problem with experiments showing very significant deviations from the initially circular shape of the drop footprint<sup>2</sup> as migration proceeds.

#### AUTHOR INFORMATION

##### Corresponding Author

Rachid Chebbi – Department of Chemical and Biological Engineering, American University of Sharjah, Sharjah 26666, United Arab Emirates; [orcid.org/0000-0003-3673-3612](https://orcid.org/0000-0003-3673-3612); Phone: 971 6 515 2983; Email: [rchebbi@aus.edu](mailto:rchebbi@aus.edu); Fax: 971 6 515 2979

Complete contact information is available at: <https://pubs.acs.org/10.1021/acsomega.3c04799>

##### Notes

The author declares no competing financial interest.

#### ACKNOWLEDGMENTS

The work in this paper was supported, in part, by the Open Access Program from the American University of Sharjah. This paper represents the opinions of the author and does not mean to represent the position or opinions of the American University of Sharjah.

#### REFERENCES

- (1) Tadmor, R. Marangoni flow revisited. *J. Colloid Interface Sci.* **2009**, *332*, 451–454.
- (2) Dai, Q.; Khonsari, M. M.; Shen, C.; Huang, W.; Wang, X. Thermocapillary migration of liquid droplets induced by a unidirectional thermal gradient. *Langmuir* **2016**, *32*, 7485–7492.
- (3) Greenspan, H. P. On the motion of a small viscous droplet that wets a surface. *J. Fluid Mech.* **1978**, *84*, 125–143.
- (4) Brochard, F. Motions of droplets on solid surfaces induced by chemical or thermal gradients. *Langmuir* **1989**, *5*, 432–438.
- (5) Brzoska, J. B.; Brochard-Wyart, F.; Rondelez, F. Motions of droplets on hydrophobic model surfaces induced by thermal gradients. *Langmuir* **1993**, *9*, 2220–2224.
- (6) Ford, M. L.; Nadim, A. Thermocapillary migration of an attached drop on a solid surface. *Phys. Fluids* **1994**, *6*, 3183–3185.

- (7) Smith, M. K. Thermocapillary migration of a two-dimensional liquid droplet on a solid surface. *J. Fluid Mech.* **1995**, *294*, 209–230.
- (8) Pratap, V.; Moumen, N.; Subramanian, R. S. Thermocapillary motion of a liquid drop on a horizontal solid surface. *Langmuir* **2008**, *24*, 5185–5193.
- (9) Huh, C.; Scriven, L. E. Hydrodynamic model of steady movement of a solid/liquid/fluid contact line. *J. Colloid Interface Sci.* **1971**, *35*, 85–101.
- (10) Dussan, V. E. B. On the spreading of liquids on solid surfaces: static and dynamic contact lines. *Annu. Rev. Fluid Mech.* **1979**, *11*, 371–400.
- (11) de Gennes, P. G. Wetting: statics and dynamics. *Rev. Mod. Phys.* **1985**, *57*, 827–863.
- (12) Blake, T. D. The physics of moving wetting line. *J. Colloid Interface Sci.* **2006**, *299*, 1–13.
- (13) Blake, T. D.; Haynes, J. M. Kinetics of liquid/liquid displacement. *J. Colloid Interface Sci.* **1969**, *30*, 421–423.
- (14) Hocking, L.; Rivers, A. The spreading of a drop by capillary action. *J. Fluid Mech.* **1982**, *121*, 425–442.
- (15) Cox, R. G. The dynamics of the spreading of liquids on a solid surface. Part 1. Viscous flow. *J. Fluid Mech.* **1986**, *168*, 169–194, DOI: [10.1017/S0022112086000332](https://doi.org/10.1017/S0022112086000332).
- (16) Brochard-Wyart, F.; de Gennes, P. G. Dynamics of partial wetting. *Adv. Colloid Interface Sci.* **1992**, *39*, 1–11.
- (17) Hervet, H.; de Gennes, P. G. Dynamique du mouillage: films précurseurs sur solides. *C. R. Acad. Sci., Ser. II* **1984**, *299*, 499–503.
- (18) Starov, V. M.; Kalinin, V. V.; Chen, J.-D. Spreading of liquid drops over dry surfaces. *Adv. Colloid Interface Sci.* **1994**, *50*, 187–221.
- (19) Chebbi, R. Dynamics of wetting. *J. Colloid Interface Sci.* **2000**, *229*, 155–164.
- (20) Singer, J. P. Thermocapillary approaches to the deliberate patterning of polymers. *J. Polym. Sci., Part B: Polym. Phys.* **2017**, *55*, 1649–1668.
- (21) Song, F.; Liu, Y.; Zhang, T.; Fan, J.; Yang, Q. Marangoni flow of thin liquid film underneath a topographical plate. *Case Stud. Therm. Eng.* **2022**, *35*, No. 102094.
- (22) Xie, J. C.; Lin, H.; Han, J. H.; Dong, X. Q.; Hue, W. R.; Hirata, A.; Sakurai, M. Experimental investigation on Marangoni drop migrations using drop shaft facility. *Int. J. Heat Mass Transfer* **1998**, *41* (14), 2077–2081.
- (23) Muñoz, J.; Arcos, J.; Bautista, O.; Méndez, F. Influence of slippage on thermocapillary flow induced by a Gaussian temperature distribution on small-scale water droplets driven by surface acoustic wave. *Wave Motion* **2023**, *120*, No. 103167.
- (24) Ma, C.; Li, C.; Xie, X.; Ye, X. On the migration of a droplet driven by thermocapillary action in a wettability-confined track. *Phys. Fluids* **2023**, *35*, No. 082104, DOI: [10.1063/5.0160390](https://doi.org/10.1063/5.0160390).
- (25) Dai, Q.; Huang, W.; Wang, X.; Khonsari, M. M. Ringlike Migration of a Droplet Propelled by an Omnidirectional Thermal Gradient. *Langmuir* **2018**, *34*, 3806–3812.
- (26) Chebbi, R. A model for the dynamics of partial wetting. *J. Chem. Eng. Jpn.* **2010**, *43*, 333–341.
- (27) Chebbi, R. Dynamics of partial wetting. *J. Adhesion Sci. Technology* **2011**, *25*, 1767–1783.
- (28) de Gennes, P. G.; Brochard-Wyart, F.; Quéré, D. *Capillarity and Wetting Phenomena: Drops, Bubbles, Pearls, Waves*; Springer: New York, 2010.